ORIGINAL ARTICLE

Probing the molecular mechanisms of α-synuclein inhibitors unveils promising natural candidates through machine-learning QSAR, pharmacophore modeling, and molecular dynamics simulations

Yassir Boulaamane[1] · Kailash Jangid[2] · Mohammed Reda Britel[1] · Amal Maurady[1,3]

Abstract

Parkinson's disease is characterized by a multifactorial nature that is linked to different pathways. Among them, the abnormal deposition and accumulation of α-synuclein fibrils is considered a neuropathological hallmark of Parkinson's disease. Several synthetic and natural compounds have been tested for their potency to inhibit the aggregation of α-synuclein. However, the molecular mechanisms responsible for the potency of these drugs to further rationalize their development and optimization are yet to be determined. To enhance our understanding of the structural requirements necessary for modulating the aggregation of α-synuclein fibrils, we retrieved a large dataset of α-synuclein inhibitors with their reported potency from the ChEMBL database to explore their chemical space and to generate QSAR models for predicting new bioactive compounds. The best performing QSAR model was applied to the LOTUS natural products database to screen for potential α-synuclein inhibitors followed by a pharmacophore design using the representative compounds sampled from each cluster in the ChEMBL dataset. Five natural products were retained after molecular docking studies displaying a binding affinity of − 6.0 kcal/mol or lower. ADMET analysis revealed satisfactory properties and predicted that all the compounds can cross the blood–brain barrier and reach their target. Finally, molecular dynamics simulations demonstrated the superior stability of LTS0078917 compared to the clinical candidate, Anle138b. We found that LTS0078917 shows promise in stabilizing the α-synuclein monomer by specifically binding to its hairpin-like coil within the N-terminal region. Our dynamic analysis of the inhibitor-monomer complex revealed a tendency towards a more compact conformation, potentially reducing the likelihood of adopting an elongated structure that favors the formation and aggregation of pathological oligomers. These findings offer valuable insights for the development of novel α-synuclein inhibitors derived from natural sources.

✉ Amal Maurady
  amal.maurady.ma@gmail.com

1 Laboratory of Innovative Technologies, National School of Applied Sciences of Tangier, Abdelmalek Essaadi University, Tetouan, Morocco
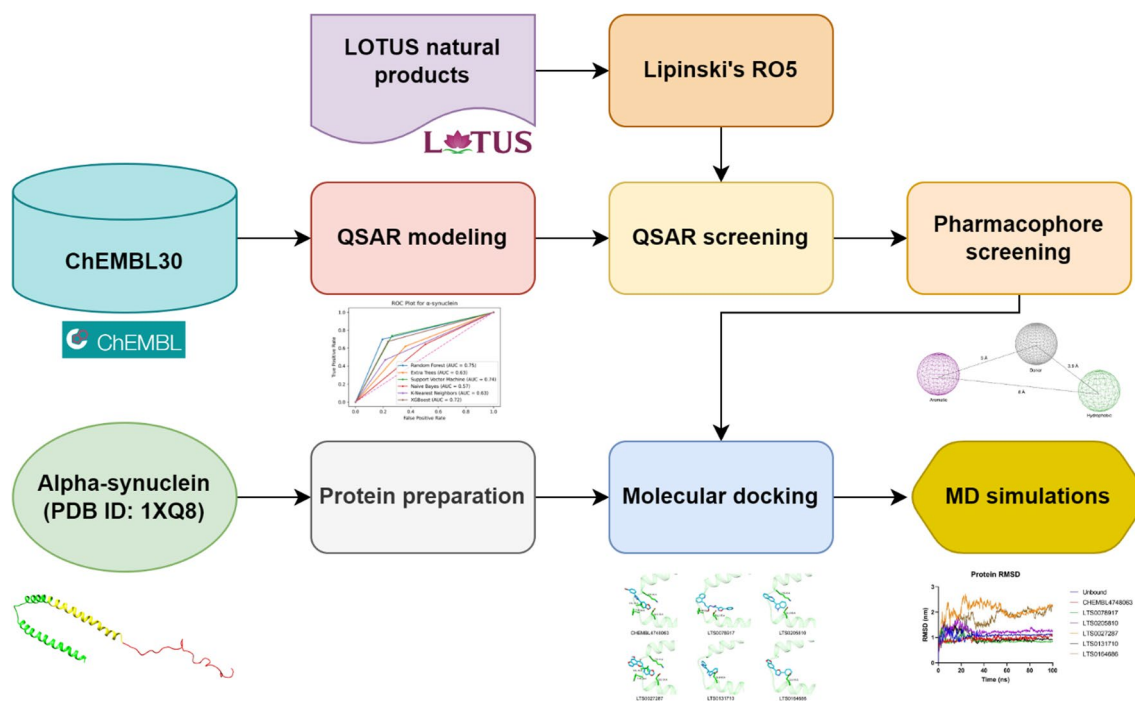
2 Department of Pharmaceutical Sciences and Natural Products, Central University of Punjab, Ghudda, Bathinda, India

3 Faculty of Sciences and Techniques of Tangier, Abdelmalek Essaadi University, Tetouan, Morocco

🖄 Springer

Graphical abstract

Keywords α-Synuclein · ADMET prediction · Machine learning · Molecular docking · Molecular dynamics simulations · Natural products · QSAR · Parkinson's disease

Introduction

Neurodegenerative disorders, including Alzheimer's and Parkinson's disease (PD), are among the most common neurological conditions globally [1]. These disorders are characterized by the gradual loss of brain cells due to a variety of factors, including the accumulation of amyloid fibrils, oxidative stress, mitochondrial dysfunction, and metal accumulation [2]. PD is the second most common neurological disorder in the world, characterized by the loss of dopaminergic neurons in the midbrain and resulting in dopamine deficiency in the striatum [3]. It is estimated to affect 6 million people globally, with a projected increase in prevalence of two- to threefold by 2030 [4, 5]. Common motor symptoms of PD include dyskinesia, tremors, and difficulty with movement [6]. Non-motor symptoms, such as depression, insomnia, and constipation, may also occur [7]. Evidence suggests that oxidative damage and mitochondrial imbalance contribute to the degeneration of dopaminergic neurons in PD [8], leading to a need for novel "disease-modifying" therapies [9]. Current treatments for PD include L-DOPA therapy, which is considered the gold standard for controlling motor symptoms, and dopaminergic treatments such as dopamine agonists, monoamine oxidase-B (MAO-B)

inhibitors, and catechol-*O*-methyltransferase (COMT) inhibitors [10, 11]. More recently, non-dopaminergic treatments, including adenosine A_{2A} and *N*-methyl-D-aspartate (NMDA) receptor antagonists, have been shown to be effective in relieving PD symptoms and slowing neuronal damage [12, 13]. Many other potential "disease-modifying" therapies are under development for PD, including agents that modulate α-synuclein, neurotrophic factors, inflammation modulators, neuroprotective agents, and multi-target drugs [14–16]. α-synuclein is a protein that is expressed in neurons of the central and peripheral nervous systems [17]. It is a member of the synuclein family of proteins, which are characterized by the presence of a central non-amyloid β component (NAC) domain and an amino-terminal domain that is rich in hydrophobic amino acids [18]. α-synuclein is thought to play a role in the regulation of neurotransmitter release and in the formation and maintenance of presynaptic terminals [19]. In PD, abnormal accumulation and aggregation of α-synuclein in the brain is believed to contribute to the degeneration of dopaminergic neurons and the development of PD symptoms [20]. The aggregation of α-synuclein can also lead to the formation of intracellular inclusions called Lewy bodies, which are a hallmark of PD pathology [21]. The precise mechanisms by which α-synuclein contributes

to the development of PD are not fully understood, but there is evidence suggesting that α-synuclein can affect the function of mitochondria, the integrity of the cytoskeleton, and the ability of cells to respond to stress [22]. A growing body of experimental evidence highlighted the potency of small molecules to inhibit the aggregation of α-synuclein fibrils. Among them, Anle138b and NPT200-11 are currently evaluated in clinical trials for their efficacy and safety. They are thought to reduce α-synuclein aggregation and misfolding, however, the molecular mechanisms behind their activity are yet to be elucidated [23, 24].

The 3D structure of α-synuclein has been resolved through solution NMR (PDB ID: 1XQ8) [25]. The snapshot represents a micelle-bound α-synuclein monomer at atomic resolution as shown in Fig. 1. The monomer is formed by 140 amino acids and has a molecular weight of approximately 14 kDA consisting of a membrane binding N-terminal region, a NAC region and an acidic C-terminal tail [26].

Previous experimental evidence revealed the molecular mechanisms of flavonoids and their anti-aggregation effects on α-synuclein, it was suggested that the binding site for small molecules is in the interhelical loop between the hairpin-like α-helices formed by the residues 30–48 [27, 28]. Several natural mutations that modify the membrane-binding affinity have been identified in this region, such as A30P and E46K, both of which are linked to distinct disease pathology [28]. Furthermore, a recent study examined the favorable binding site between α-synuclein and Quercetin, a flavonoid found in many fruits, vegetables, leaves, seeds, and grains. They found that Quercetin binds near the lysine-rich region formed by the residues: LYS-32, LYS-43, LYS-45, and VAL-40 [29]. The effectiveness of Quercetin and its oxidized form against α-synuclein fibrillization has been demonstrated in many in vitro assays and neuron-like PC12 cell models [30, 31]. When Quercetin interacts with early-stage aggregates, they result in highly soluble α-synuclein oligomers. This occurs because the polyphenol binds to the lysine side chains located in the N-terminal domain of α-synuclein [32].

In the present study, a dataset of experimentally evaluated α-synuclein inhibitors was retrieved from the ChEMBL database (https://www.ebi.ac.uk/chembl/) [33] and was employed to develop quantitative structure–activity relationship (QSAR) models to screen for novel potential α-synuclein inhibitors. Exploratory data analysis was performed to define the chemical space of bioactive inhibitors and cluster similar compounds. The best performing QSAR model was selected to screen for natural products as potential α-synuclein inhibitors. Moreover, a pharmacophore was generated from the representative experimental drugs and was used to further screen our dataset. A molecular docking study was conducted on the remaining compounds to evaluate the molecular interactions involved in the ligand binding. Subsequently, an ADMET analysis was conducted to evaluate the suitability of the compounds to act as central nervous system (CNS) drugs. Finally, 100 ns molecular dynamics (MD) simulations were conducted to assess the stability of α-synulcein in the unbound state and when bound to the reference inhibitor and the selected natural products.
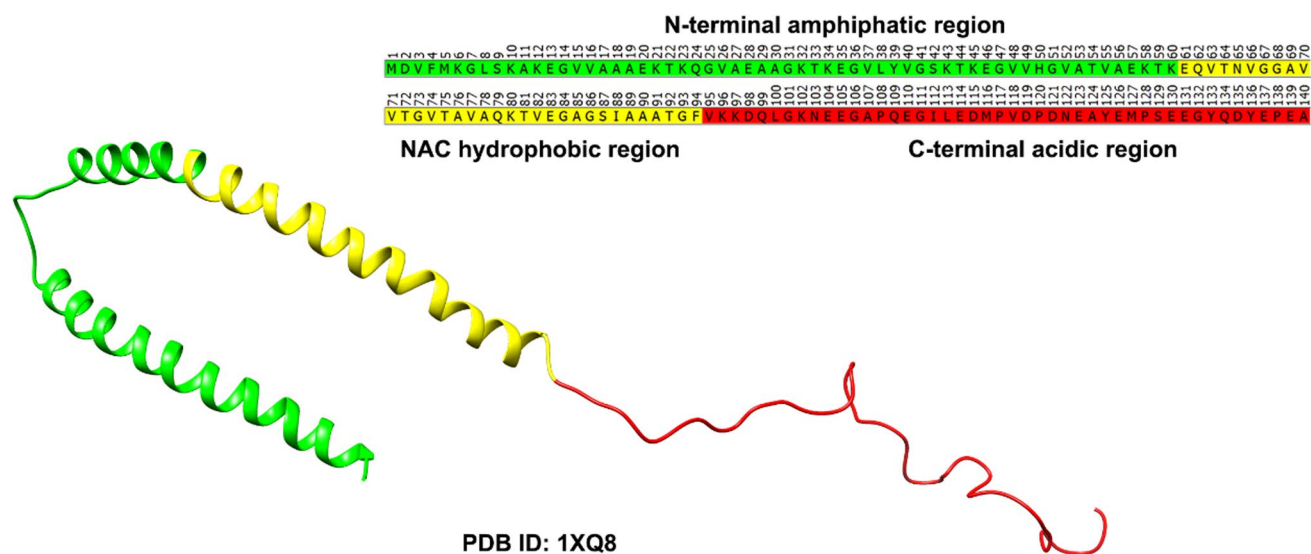

Fig. 1 Micelle-bound α-synuclein monomer solved by solution NMR (PDB ID: 1XQ8) and the corresponding full sequence. The structure is formed by three domains: N-terminal, NAC, and C-terminal region

Materials and methods

Bioactivity dataset preparation

A bioactivity dataset was retrieved from the ChEMBL database containing chemical structures of 10,408 compounds with their reported potency against human α-synuclein [33]. The dataset was curated by removing duplicate compounds. The molecules were classified as either "active" or "inactive" according to the information provided in the ChEMBL dataset. Compounds with "inconclusive" labels were omitted from the study. The processed dataset contained 524 compounds labelled as "active" and 3755 labelled as "inactive". To obtain a more balanced classification, inactive compounds were clustered using Tanimoto similarity coefficient [34]. The final dataset contained 1124 compounds where 524 are "active" and 600 are "inactive".

QSAR modelling

The final dataset was used to generate 2048 bits of circular molecular descriptors using Morgan fingerprints included in the RDKit cheminformatics suite with a Radius value of 2 based on the popular extended-connectivity fingerprints (ECFP4) derived from the SMILES representations of the compounds in the dataset [35, 36]. Datasets were split into training and testing sets using the 70/30 rule. The testing set was subject to an additional 80/20 split into testing and validation sets before building the QSAR models as illustrated in Fig. 2. Various statistical metrics were used to assess the performance of the machine learning models. To evaluate the classification ability, parameters such as true positive

rate (TPR) (Eq. 1), true negative rate (TNR) (Eq. 2), false positive rate (FPR) (Eq. 3), false negative rate (FNR) (Eq. 4), accuracy (ACC) (Eq. 5), and Matthews correlation coefficient (MCC) (Eq. 6) were calculated using the following equations:

$$TPR = \frac{TP}{(TP + FN)} \tag{1}$$

$$TNR = \frac{TN}{(FP + TN)} \tag{2}$$

$$FPR = \frac{FP}{(FP + TN)} \tag{3}$$

$$FNR = \frac{FN}{(FN + TP)} \tag{4}$$

$$ACC = \frac{(TP + TN)}{(P + N)} \tag{5}$$

$$MCC = \frac{(TP \times TN) - (FP \times FN)}{\sqrt{(TP + FP) * (TP + FN) * (TN + FP) * (TN + FN)}} \tag{6}$$

Natural products dataset preparation

The chemical structures of natural products were obtained from the LOTUS database in SMILES format. The database contains more than 200,000 distinct compound names and structural elements, as well as over 500,000 records of
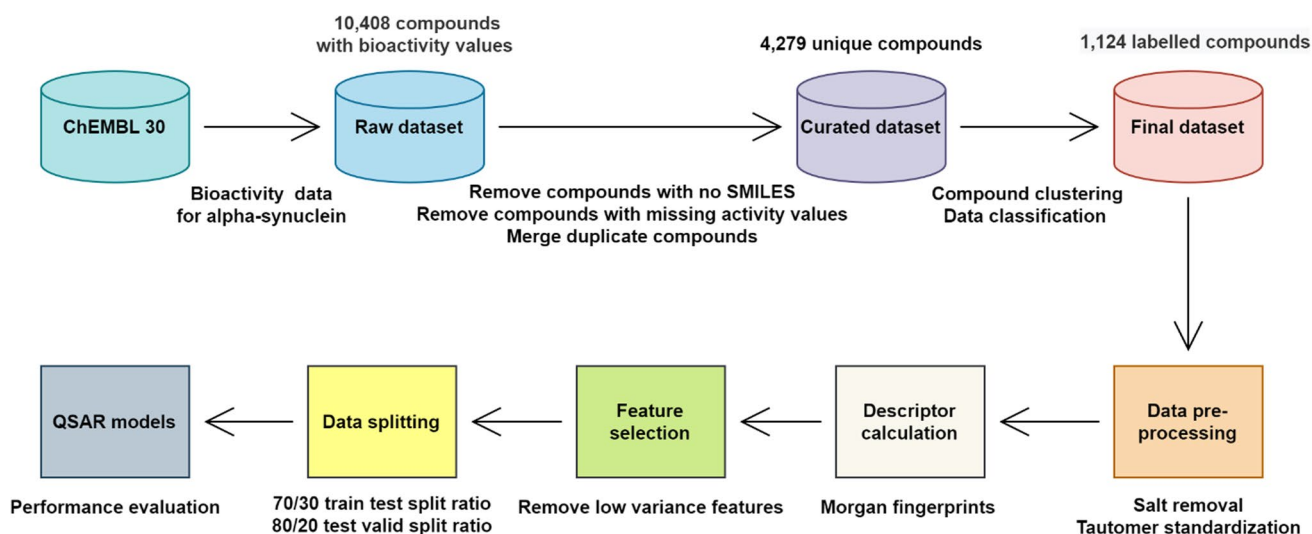

Fig. 2 Machine learning-based QSAR modelling workflow for α-synuclein inhibitors reported in the ChEMBL database

distinct, fully cited structure-organism pairs [37]. The structures were filtered using Lipinski's rule of five to remove any compounds that did not meet the criteria for orally active drugs [38]. The remaining compounds were analyzed using the DataWarrior Cheminformatics program to generate their 2D structures and calculate their physicochemical properties [39]. Only compounds with properties within the recommended range for orally active drugs were retained and saved in a CSV file for subsequent use in QSAR bioactivity prediction.

Pharmacophore modelling

To minimize the number of compounds for molecular docking experiments and ensure that only those meeting the essential pharmacophoric prerequisites present in clinical candidates were considered, we employed the Pharmit webserver (https://pharmit.csb.pitt.edu/) [40]. Using the clinical candidate Anle138b as a reference, we constructed our pharmacophore with the help of Pharmit. The pharmacophore was subsequently employed to screen the natural products that had been predicted to be bioactive through our QSAR study. The remaining compounds were then subjected to molecular docking investigations.

Molecular docking

The solution NMR structure of α-synuclein monomer was retrieved from the RCSB PDB (https://www.rcsb.org/) with PDB ID: 1XQ8 [25]. Polar hydrogens and Kollman charges were added using AutoDockTools 1.5.6 [41]. The C-terminal tail was omitted from the study to ease the calculation charge and the resulting protein was used for molecular docking, without any further adjustment. The binding site druggability was assessed using DoGSiteScorer which is a grid-based method that uses a Difference of Gaussian filter to detect potential binding pockets solely based on the 3D structure of the protein [42, 43]. The highest-scoring pocket (Drug Score = 0.55) was found to be in the interhelical loop between the two α-helices as mentioned in the literature [27, 28]. The grid box was centered around this region formed by residues 30–48 of α-synuclein with the coordinates: − 12.29 x − 24.50 x − 82.36 in x, y, and z directions respectively with a box size of 24 Å and a spacing of 1 Å. The binding site of α-synuclein and its residues is shown in Fig. 3.

Molecular docking was performed using AutoDock Vina 1.1.2 [44]. Since there is no reference ligand in the protein structure, the best docking poses were chosen according to their binding affinity and molecular interactions [45]. Protein–ligand interactions such as hydrogen bonds and hydrophobic interactions were visualized using the Protein–Ligand Interaction Profiler (PLIP) web tool (https://plip-tool.biotec.tu-dresden.de/plip-web/plip/index) [46].

ADMET analysis

ADMET stands for Absorption, Distribution, Metabolism, Excretion, and Toxicity. These are the key factors that determine the potential of a drug candidate to be developed into a safe and effective medicine [47]. In silico ADMET prediction is the use of computer-based methods to predict the potential of a chemical compound to be absorbed,
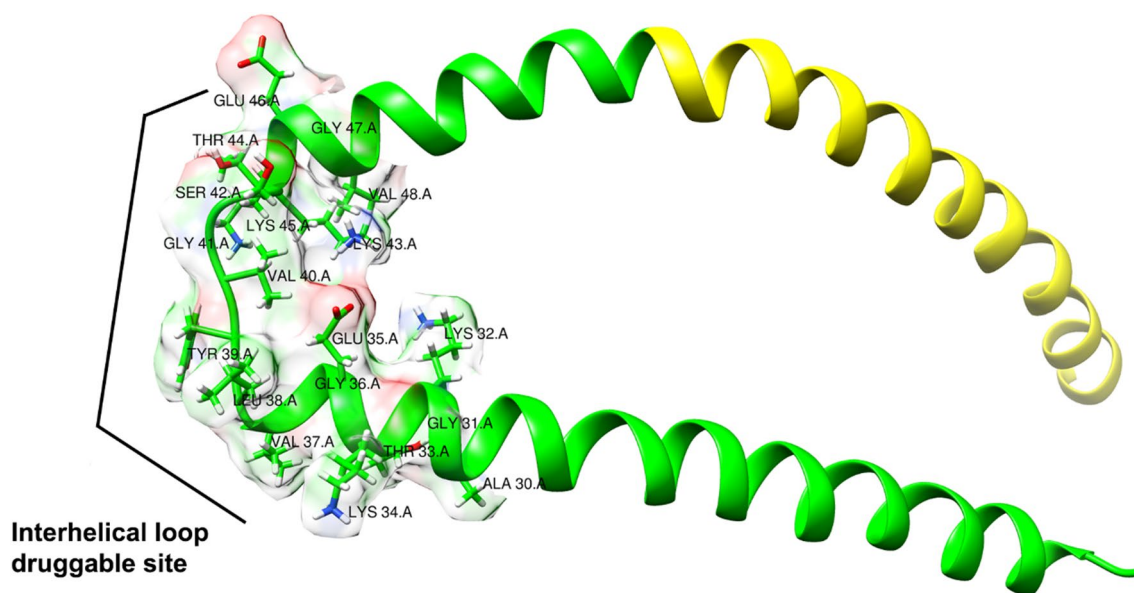

Fig. 3 Binding site of α-synuclein monomer at the interhelical loop located in the N-terminal region (PDB ID: 1XQ8)

distributed within the body, metabolized, excreted, and cause toxicity in living organisms [48]. ADMET prediction is an important tool in the early stages of drug discovery and development, as it allows researchers to identify potential compounds with favorable ADMET properties, reducing the need for costly and time-consuming animal testing [49]. In this study, pkCSM webserver (https://biosig.lab.uq.edu.au/pkcsm/) [50] was used to compute various parameters such as water solubility to determine how easily a drug can dissolve in the body and be absorbed into the bloodstream, intestinal absorption which refers to the extent to which a drug is absorbed into the body through the gastrointestinal tract, blood–brain barrier (BBB) permeability refers to the ability of a drug to pass through the BBB and reach the CNS, CYP2D6 interaction refers to the potential of a drug to interact with the enzyme CYP2D6, which is involved in the metabolism of many drugs [51]. Ames toxicity is a type of genotoxicity assessment used to determine the mutagenic potential of a compound, specifically its ability to cause mutations in bacteria whereas hepatotoxicity refers to the potential of a drug to cause injuries to the liver's normal function [45].

Molecular dynamics simulations

The stability of the selected candidates with respect to the binding site of α-synuclein monomer was determined using MD simulations with GROMACS 2021.3 [52, 53]. The protein structure of α-synuclein was prepared using CHARMM-GUI webserver [54]. The CHARMM36 all-atom force field was used to generate the protein topology file with the pdb2gmx module of GROMACS. Meanwhile, the CGENFF server (https://cgenff.umaryland.edu/) was used to assign atom types and bonded parameters and charges to the ligands [55]. The generated ligand files were then translated to GROMACS topology files using cgenff_charmm2gmx python script [56]. Subsequently, the TIP3P water model was chosen to solvate the protein–ligand systems in a cubic box of size $150 \times 80 \times 80$ in x, y, and z directions respectively. Na^+ and Cl^- ions were added to neutralize the system charge. All the systems were simulated in the standard biological salt concentration of 0.15 mM. For energy minimization, the steepest descent technique was utilized, with Fmax set to not exceed 1000 kJ/mol/nm. Two successive 1 ns simulation using canonical NVT, and isobaric NPT ensembles were used to equilibrate the system at 300 Kelvin and a pressure of 1 bar. All the simulations were carried out under periodic boundary conditions (PBC), and long-range electrostatic interactions were treated using the particle mesh Ewald method [57]. Finally, 100 ns MD simulations were then performed for data collection [58–60]. Various geometrical properties were calculated using GROMACS program to analyze the dynamic behavior of the selected
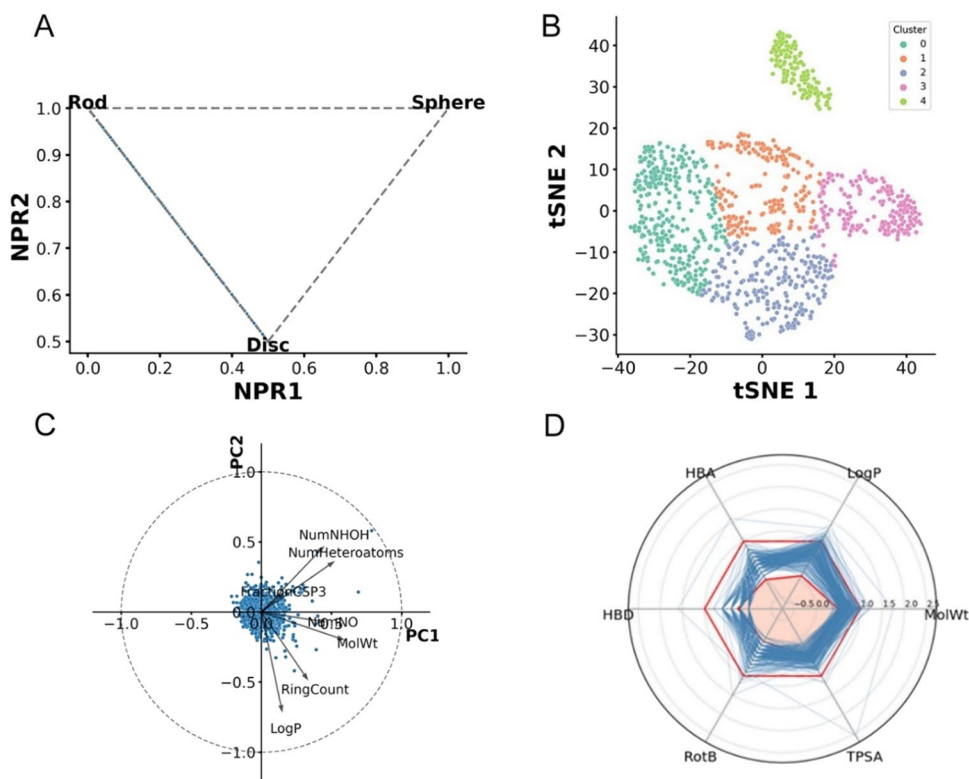
complexes such as root-mean square deviation (RMSD), root-mean square fluctuation (RMSF), radius of gyration (Rg), solvent accessible surface area (SASA), principal component analysis (PCA), and hydrogen bonds [61].

Results and discussion

Chemical space of α-synuclein inhibitors

Chemical space diversity of a dataset is important for the performance of machine learning classification models because a diverse set of compounds helps to prevent chemical sampling bias and leads to higher prediction accuracy and stronger generalization ability of the models. The chemical space diversity of the α-synuclein dataset was analysed using the Normalized principal moment of inertia ratios (NPR) plot to analyse the shape and size of molecules [62]. The normalized PMI ratios were then plotted on a triangular graph, where the vertices (0,1), (0.5,0.5), and (1,1) represent a perfect rod (2-butyne), disc (benzene), and sphere (adamantane), respectively (Fig. 4A). Each molecule is represented by a single point in a three-dimensional space, with the x, y, and z axes corresponding to the normalized principal moment of inertia (PMI) for the three principal axes of the molecule (I_{xx}, I_{yy}, I_{zz}). The distance of the point from the origin of the plot represents the size of the molecule, while the orientation of the point reflects the shape of the molecule. Notably, all the studied α-synuclein inhibitors occupied the rod-disc region of the graph characterized by high values of NPR1 (I_2/I_1) and NPR2 (I_3/I_1). High NPR1 values suggest that the molecules have an elongated or rod-like shape, while high NPR2 values indicate a flattened or disc-like shape. This observation indicates that the molecules exhibit a common structural feature of elongation and a tendency toward planarity. T-Distributed Stochastic Neighbor Embedding (t-SNE) is a popular plot for visualizing high-dimensionality data while preserving the distances between the points as much as possible. In Fig. 4B, t-SNE analysis was used to compare molecules by their structural features based on RDkit's Morgan fingerprints [63]. To identify cluster of compounds with similar features, we employed k-means clustering method [64]. Then, we determined the optimal number of clusters using the silhouette-based algorithm [65]. The silhouette score is a metric commonly used to assess the effectiveness of clustering techniques [66]. Despite the average silhouette score for the five identified clusters was 0.26 which is considerate fair, the selected diverse set of representative compounds for molecular docking from each cluster represent compounds with different scaffolds. The lack of separation could be due to the dimensionality reduction resulting in some overlapping regions between clusters. Finally, principal component analysis (PCA) was performed

to analyze the physicochemical properties of the molecules (Fig. 4C) [67]. By examining the correlations with PC1 (TPSA, HBA, MolWt) and PC2 (HBD, nRotB, LogP), we can identify the features that have positive and negative associations. Notably, LogP stands out as the "most important" feature (descriptor) due to its vector length. Finally, the radar chart of beyond Lipinski's rule of five (bRo5) was performed to assess the percentage of the compounds that are unlikely to be suitable for oral administration [68]. Figure 4D illustrates that the majority of compounds in the dataset adhere to the suggested ranges for physicochemical properties as defined by Lipinski's rule of five.

Validation of the QSAR models

Six machine learning (ML) algorithms that are known to perform well for QSAR modeling such as Random Forest (RF), Support Vector Machine (SVM), k-Nearest Neighbors (kNN), Extra Trees (ET), Gaussian Naïve Bayes (GNB), and XGBoost (XGB) were selected to build our models [69]. The receiving operating characteristic (ROC) curve was used to evaluate the quality of the developed QSAR classification models by comparing the true positive rate to the false positive rate. After evaluating the six QSAR models, we identified that the RF algorithm yielded the highest performance. The QSAR model based on the RF algorithm achieved an area under the ROC curve (AUC) value of 0.75 (Fig. 5) for the testing set and 0.72 for the external validation set for
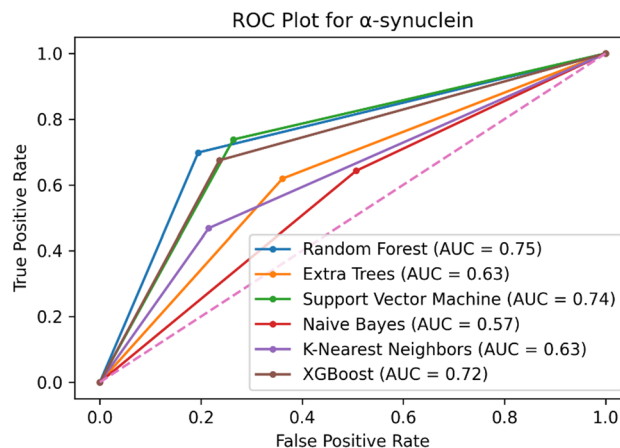

Fig. 5 ROC plot for α-synuclein visualizing the trade-off between true positive and false positive rates

α-synuclein inhibitors. This indicates a reasonably good predictive ability of the model in distinguishing between positive and negative instances. The performance of all the QSAR models was also assessed using various performance metrics, as shown in Table 1.

The best performing QSAR model based on the RF algorithm was then applied to the LOTUS dataset containing 129,557 natural products to screen for potential α-synuclein inhibitors. 40,251 compounds were retained at this stage and were subjected to a pharmacophore-based virtual screening.

Table 1 Comparing the performance of multiple machine learning models using a variety of statistical metrics

ML model	Testing set							Validation set
	TPR	TNR	FPR	FNR	ACC	MCC	AUC	AUC
Random forest	0.75	0.75	0.24	0.24	0.75	0.51	0.75	0.72
Support vector machine	0.76	0.70	0.29	0.23	0.73	0.47	0.74	0.71
k-nearest neighbors	0.62	0.65	0.34	0.37	0.63	0.27	0.62	0.66
Extra trees	0.65	0.60	0.4	0.34	0.62	0.25	0.62	0.65
Gaussian Naïve Bayes	0.61	0.52	0.47	0.38	0.56	0.13	0.56	0.53
XGBoost	0.72	0.71	0.28	0.27	0.72	0.44	0.72	0.71

Fig. 6 Pharmacophoric features selected based on the clinical candidate, Anle138b using Pharmit server
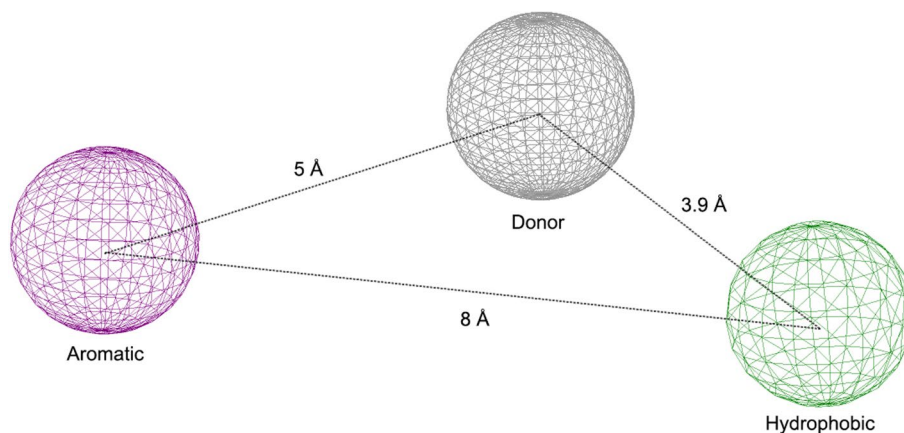

Pharmacophore screening

Prior research has emphasized the significance of the nitrogen atoms located in the imidazole ring of the clinical candidate Anle138b (CHEMBL4748063) in establishing a hydrogen bond with VAL-40 of the interhelical loop in α-synuclein [28]. Using the existing literature and Anle138b's chemical structure, we have devised a pharmacophore model that enables us to narrow down the pool of compounds and only retain those exhibiting the desired pharmacophoric traits as depicted in Fig. 6.

The pharmacophore model we created contained an aromatic ring, a hydrophobic component, and a hydrogen donor group in the center. This is consistent with earlier research that attempted to develop a pharmacophore model for α-synuclein inhibitors [70, 71]. After employing our pharmacophore for screening, we were able to identify 103 compounds that met the proposed criteria out of a total of 40,251 compounds. These compounds were then subjected to molecular docking investigations.
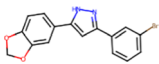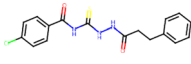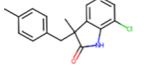
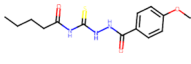## Molecular docking of α-synuclein inhibitors
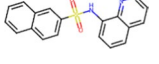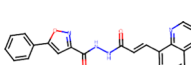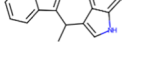
A molecular docking study was conducted for the experimental α-synuclein inhibitors as well as the remaining natural products against the binding site of the target monomer. The best docking poses were selected according to their
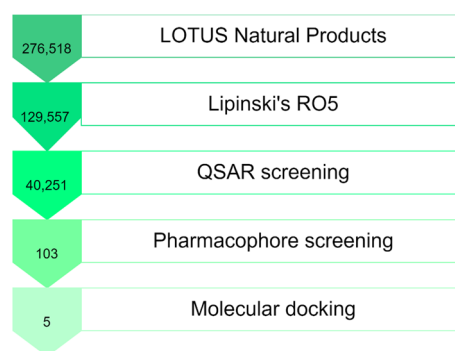
Fig. 7 Virtual screening workflow used in this study to screen for potential α-synuclein inhibitors from natural products

binding affinity and their protein–ligand interactions. Only five compounds were retained displaying a binding energy of − 6.0 kcal/mol or lower as illustrated in Fig. 7. The molecular doc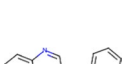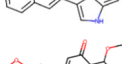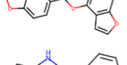king results of the highest-ranking candidates, their chemical structures and their molecular interactions are shown in Table 2. The best docking poses were visualized using UCSF Chimera software [72] and are shown in Fig. 8.

The selected compounds showed low binding affinity when docked against the interhelical region of α-synuclein, in contrast to other macromolecules such as enzymes and receptors with well-defined binding cavities. However, the binding scores, ranging from − 6.0 to − 6.6 kcal/mol, were

Table 2 Molecular docking and protein–ligand interactions of α-synuclein inhibitors and the identified natural products

Compound	Chemical structure	Docking score (kcal/mol)	Hydrogen bonds	Distance (Å)	Hydrophobic interactions
CHEMBL4748063		− 6.2	VAL-40	1.9	TYR-39 VAL-40 LYS-43 THR-44 LYS-45
CHEMBL1544679		− 6.1	LYS-43	2.0	GLU-35 VAL-40 LYS-43
CHEMBL2133766		− 6.0	LYS-45	2.5	GLU-35 VAL-40 LYS-43
CHEMBL1299242		− 5.9	VAL-40	3.3	GLU-35 TYR-39 VAL-40 LYS-43
CHEMBL3392484		− 5.2	VAL-40	2.5	GLU-35 VAL-40 LYS-43 VAL-48
			LYS-43	2.4	
			LYS-43	2.7	
LTS0078917		− 6.6	GLU-35	3.4	LYS-32 TYR-39
			LEU-38	1.9	
			LYS-43	3.3	
LTS0205810		− 6.5	GLU-35	2.1	GLU-35 TYR-39 LYS-43
LTS0027287		− 6.2	LYS-45	3.5	TYR-39 VAL-40 LYS-43
LTS0131710		− 6.2	GLU-35	2.2	GLU-35 TYR-39 LYS-43 THR-44
			VAL-40	2.5	
LTS0164686		− 6.0	LYS-45	3.4	GLU-35 TYR-39 LYS-43

consistent with other molecular docking studies against α-synuclein that have been reported in literature [73, 74].

ADMET evaluation results

The studied molecules were subjected to an in silico ADMET analysis to assess their suitability as drugs acting on the brain as shown in Table 3. All the compounds demonstrated a good water solubility with LogS values ranging from − 3.4 to − 4.9, and displayed high intestinal absorption (> 90%). Furthermore, all compounds were predicted to have the ability to cross the BBB. Importantly, none of the compounds were identified as substrates of CYP2D6, an enzyme predominantly expressed in the brain that metabolizes endogenous neural compounds with potential neuroprotective effects [75]. Additionally, based on the Ames toxicity prediction results, five compounds, including four natural products, were predicted to be mutagenic. Furthermore, the assessment of hepatotoxicity indicated that four compounds could potentially cause liver injury and disrupt its normal function. Notably, among the predicted toxic compounds, the clinical candidate Anle138b was included, underscoring

the necessity for experimental toxicity studies to confirm its safety.

Molecular dynamics analysis

Following the analysis of molecular docking results, the clinical candidate Anle138b (CHEMBL4748063) along with the selected natural products were chosen for 100 ns MD simulations. Additionally, the unbound state of the α-synuclein monomer was included to evaluate and compare its stability with the complexes throughout the entire simulation period.

Root-mean square deviation

During the molecular docking study, the protein structure was considered rigid. To better understand the interactions between the protein and the ligands, MD simulations of the docked complexes were conducted in a water environment for a duration of 100 ns. The RMSD was calculated relative to the solution NMR protein of the targeted α-synuclein structure (PDB ID: 1XQ8) in complex with the selected candidates. Figure 9 displays RMSD values for both the protein
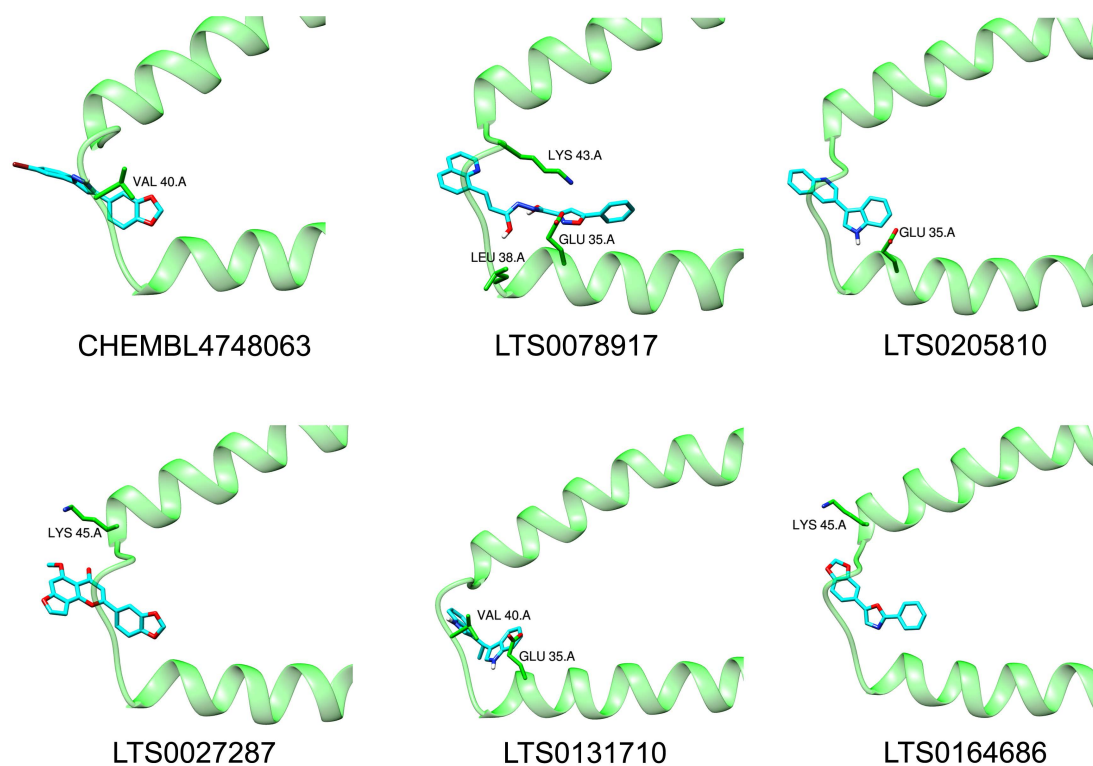
Fig. 8 Molecular docking conformations of the reference inhibitor Anle138b and the selected natural products when bound to α-synuclein

Table 3 ADMET prediction results for the selected compounds

Compound	Water solubility	Intestinal absorption	BBB permeability	CYP2D6 substrate	Ames toxicity	Hepatotoxicity
CHEMBL4748063	− 3.4	92.1	0.4	No	No	Yes
CHEMBL1544679	− 4.6	90.2	− 0.7	No	No	No
CHEMBL2133766	− 4.9	91.6	0.6	No	Yes	No
CHEMBL1299242	− 3.4	92.6	− 0.7	No	No	No
CHEMBL3392484	− 4.7	94.5	0.4	No	No	Yes
LTS0078917	− 4.7	97.2	− 0.8	No	No	Yes
LTS0205810	− 4.6	96.0	0.4	No	Yes	Yes
LTS0027287	− 4.3	99.7	− 0.7	No	Yes	No
LTS0131710	− 3.9	92.5	0.7	Yes	Yes	Yes
LTS0164686	− 4.0	96.5	0.3	No	Yes	No

Water solubility: Solubility of the molecule in water at 25 °C (log mol/L); Intestinal absorption: Percentage that will be absorbed through the human intestine; BBB permeability: Logarithmic ratio of brain to plasma drug concentrations. ($\log BB > 0.3$ is considered to cross the BBB while molecules with $\log BB < -$ 1 are poorly distributed to the brain; CYP2D6 substrate: Likeliness of a drug to be metabolized by the cytochrome P450; Ames toxicity: Likeliness of a compound to be mutagenic; Hepatotoxicity: Likeliness of drug-induced liver injury

backbone and the bound ligands, plotted against simulation time for each protein.

The RMSD analysis indicated that the majority of the complexes exhibited deviations ranging from 1 to 2 nm within the first 20 ns of the simulation. By the 40 ns mark, most complexes had reached equilibrium with RMSD values stabilizing around 1 nm. However, LTS0027287 and LTS0164686 showed larger deviations exceeding 2 nm, suggesting significant conformational changes. Notably, LTS0078917 demonstrated the highest stability throughout
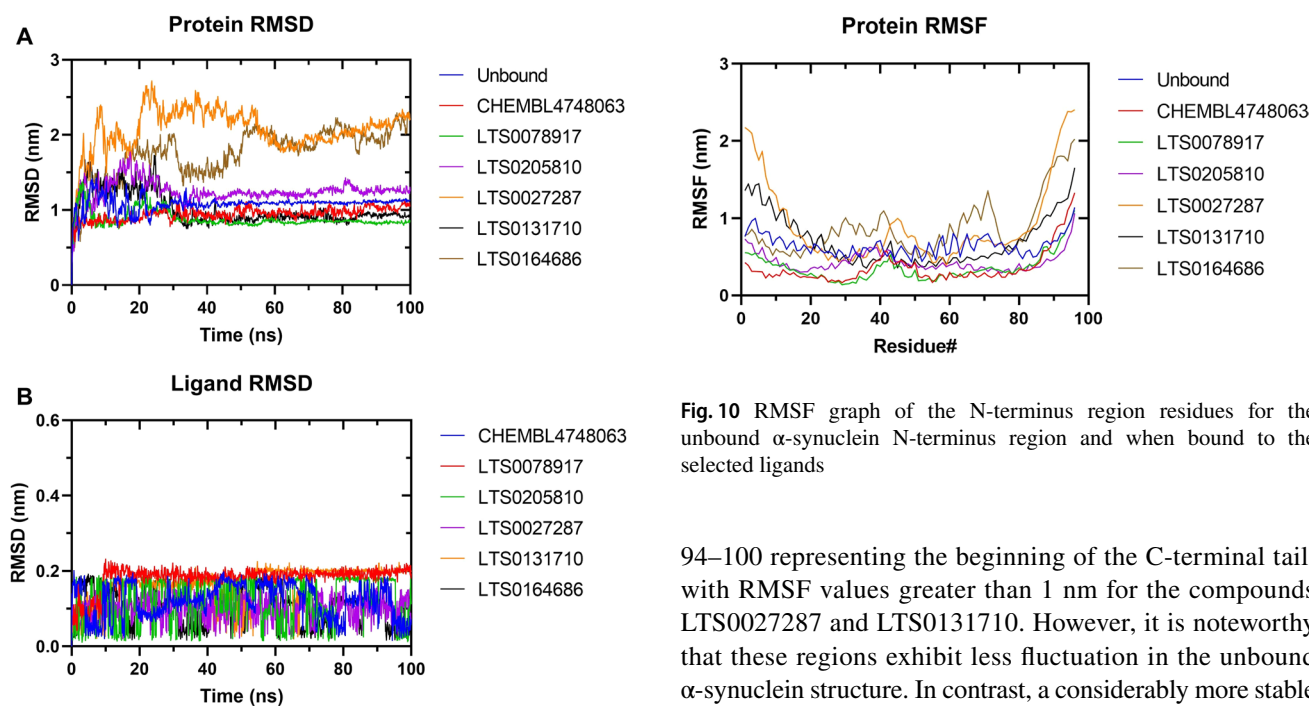
A — Protein RMSD

B — Ligand RMSD

Fig. 9 RMSD graphs of the backbone atoms of α-synuclein in complex with the selected ligands (**A**) and for the heavy atoms of the selected ligands with respect to the protein (**B**)

Protein RMSF

Fig. 10 RMSF graph of the N-terminus region residues for the unbound α-synuclein N-terminus region and when bound to the selected ligands

the simulation, maintaining an RMSD value of 0.8 nm over the entire simulation duration.

The ligand RMSD is a measure of the structural variability of a molecule during a simulation [76]. The analyzed natural products exhibited a narrow range of fluctuation in RMSD values, spanning from 0 to 0.2 nm. This implies that these ligands may undergo minor conformational changes due to their inherent flexibility. In contrast, LTS0078917 adopted a stable conformation within the initial 10 ns and maintained a significantly more stable RMSD value of approximately 0.2 nm throughout the remainder of the simulation. These results indicate that LTS0078917 exhibits lower structural variability compared to the other ligands and is likely to retain a consistent conformation throughout the simulation duration.

Root-mean square fluctuation

The RMSF is a measure of a protein's flexibility during molecular simulations, revealing the level of flexibility in different regions of the protein by calculating the motion of each residue around the average position [77]. Figure 10 shows the RMSF profile for the selected complexes, indicating that the binding of these inhibitors has a similar impact on the pattern of residue fluctuations in the protein. The regions with the highest fluctuations were found in residues 0–5 located at the extremity of the N-terminal and
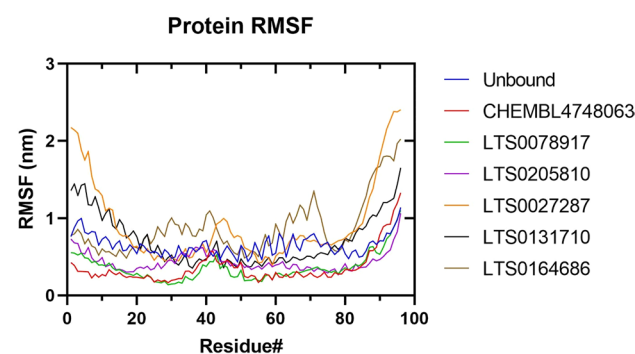
94–100 representing the beginning of the C-terminal tail, with RMSF values greater than 1 nm for the compounds LTS0027287 and LTS0131710. However, it is noteworthy that these regions exhibit less fluctuation in the unbound α-synuclein structure. In contrast, a considerably more stable RMSF was observed in the presence of the clinical candidate CHEMBL4748063 and LTS0078917. This observation suggests that these compounds potentially exert a stabilizing effect on the protein, reducing the fluctuations in these regions. Furthermore, the RMSF analysis revealed that the residues surrounding the ligand in the binding pocket exhibited RMSF values less than 1 nm, suggesting a stable binding pocket. However, notable peaks in RMSF were observed for residues 40–44, which consist of VAL-40, GLY-41, SER-42, LYS-43, and THR-44. These particular residues are known to be among the most flexible amino acids, indicating their inherent mobility even within the binding pocket.

Radius of gyration

Rg is a metric used to assess the size and shape of biomolecular structures, such as proteins. It is calculated by measuring the root-mean-square distance of all atoms in the structure from the center of mass. In the context of this study, the Rg values for the protein in complex with CHEMBL4748063, LTS0078917, and LTS0131710 were found to be consistently stable, with values approximately 2.4 nm. This is in contrast to the unbound structure, which exhibited an Rg value of 2.8 nm, as depicted in Fig. 11. The observed stability in Rg suggests that the binding of these compounds to the protein may contribute to a more compact and restrained conformation compared to the unbound state. In contrast, when the protein was bound to LTS0205810, fluctuations in the Rg were observed, leading to higher values reaching approximately 2.8 nm. Whereas the protein completely lost its compactness when bound to LTS0027287 resulting in a higher Rg reaching a value of
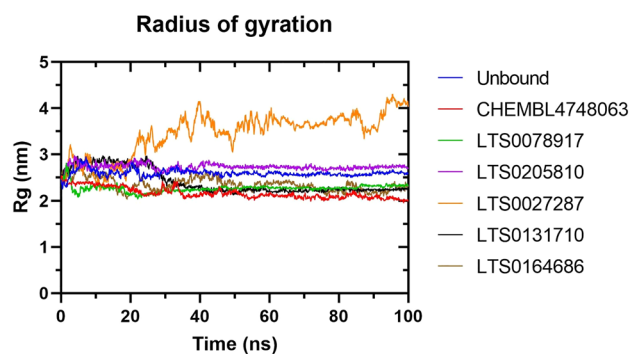
Radius of gyration

Fig. 11 Radius of Gyration of α-synuclein in unbound and bound states

A

Solvent accessible surface
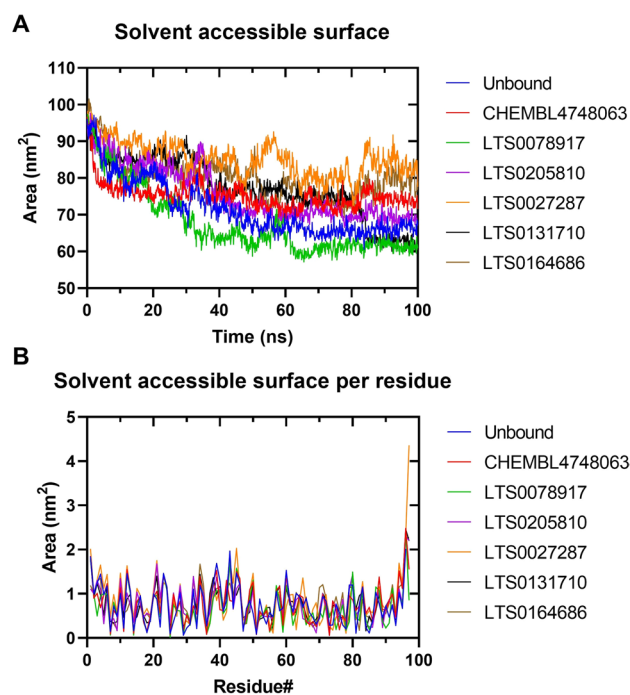

B

Solvent accessible surface per residue

Fig. 12 Solvent accessible surface area for the studied complexes over the simulation time (**A**) and per residue analysis for each complex (**B**)

4 nm and still increasing. This suggests that the binding of LTS0027287 causes a change in the shape of the protein leading to a more extended conformation which favors the formation and aggregation of pathologic oligomers.

Solvent accessible surface

The SASA is a measure of the exposed area of proteins that is accessible to solvent molecules, providing information about their relative exposure or burial within the protein structure [78]. In Fig. 12, the SASA plots for the α-synuclein complexes depict changes over the simulation time and on

a per-residue basis. The analysis reveals a consistent trend of decreasing SASA values over time for all complexes. Notably, compared to the unbound state of α-synuclein, the protein–ligand complexes exhibit increased SASA values, indicating greater exposure to solvent molecules. Interestingly, the compound LTS0078917 stands out as it exhibits the lowest SASA value among the complexes, suggesting a more compact or buried conformation with reduced solvent exposure. This could imply stronger interactions or a tighter binding of LTS0078917 with α-synuclein, leading to a more constrained and less exposed protein–ligand complex.

On the other hand, the analysis of SASA per residue consistently demonstrated a similar trend across all the complexes, where the calculated area values ranged from 1 to 2 nm^2. These values are considered very low, indicating the hydrophobic nature of these regions. Notably, the C-terminal acidic region exhibited the highest solvent exposure among the residues, which is associated to its hydrophilic properties.

Principal component analysis

PCA is a technique used to analyze the motion of biomolecular systems in a molecular dynamics simulation [79]. It identifies the dominant modes of motion by extracting eigenvectors and eigenvalues from the trajectory data. These eigenvectors and eigenvalues describe the principal components and their amplitudes, respectively, capturing the internal motions within a protein [80]. In our study, we employed PCA to investigate conformational changes in the selected complexes. Specifically, we focused on the backbone atoms and analyzed the motions associated with the principal components (PCs).

Since the first few eigenvectors adequately describe most of the internal motions in a protein, we selected the first 40 eigenvectors to calculate the concerted motions in the final 50 ns of the trajectory. Figure 13A illustrates the eigenvalues obtained by diagonalizing the covariance matrix of atomic fluctuations. The eigenvalues are ordered in decreasing magnitude and correspond to their respective eigenvectors. For the last 50 ns of the trajectories, the first ten eigenvectors account for 52.62%, 95.06%, 94.72%, 78.71%, 78.05%, and 72.21% of the motions in CHEMBL4748063, LTS0078917, LTS0205810, LTS0027287, LTS0131710, LTS0164686 complexes, respectively. Another approach to visualizing the dynamics of the complexes is by generating a 2D projection plot using PCA. The first PC1 captures the most variance in the data, followed by PC2 and subsequent components. Therefore, we utilized PC1 and PC2 of the backbone atoms to create a projection of the entire dataset in a lower-dimensional space suitable for 2D visualization. Figure 13B presents the projection of the two selected eigenvectors for all complexes. It is known that complexes occupying a smaller
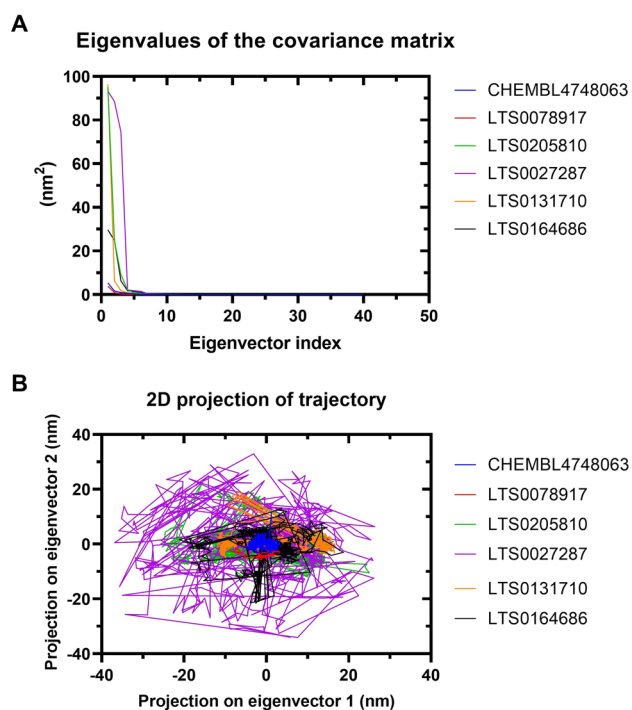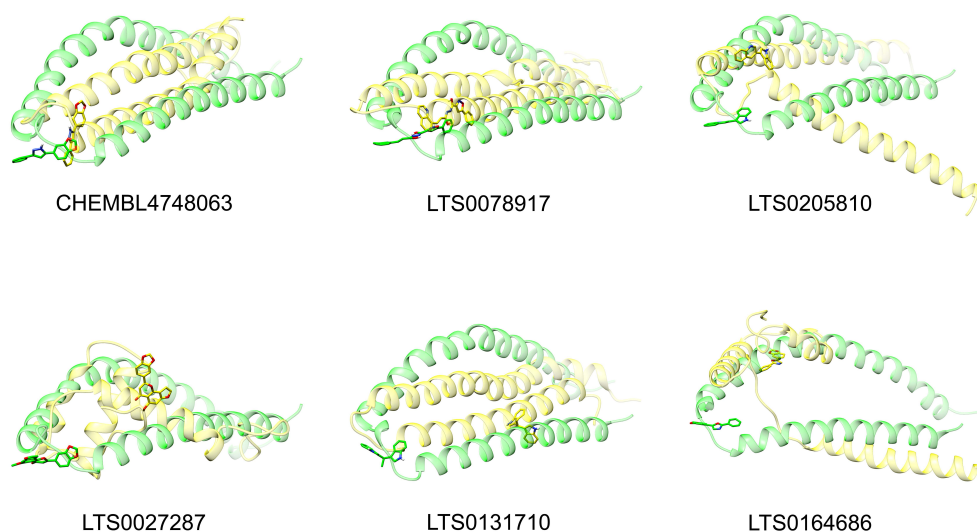
A

B

Fig. 13 Plot of the eigenvalues of the covariance matrix against the first 40 eigenvectors (**A**). 2D motion projection of α-synuclein backbone bound to the selected compounds using first two eigenvectors (**B**)

to other complexes. On the other hand, CHEMBL4748063 and LTS0078917 occupied a smaller phase space and demonstrated a stable cluster.

In Fig. 14, we presented snapshots of the initial conformations superposed with the final conformations at 100 ns, shedding light on the dynamics of the protein–ligand complexes. Our findings reveal that certain complexes underwent significant conformational changes, resulting in the disruption of ligand binding to the interhelical loop region. Notably, LTS0205810, LTS0027287, and LTS0164686 showed the most pronounced alterations in their binding modes. Conversely, the complexes formed by CHEMBL4748063 and LTS0078917 displayed a more compact and stable conformation, suggesting their potential as stabilizers of the α-synuclein monomer. This observation highlights their promising role in mitigating the aggregation and oligomerization of α-synuclein fibrils.

Hydrogen bonds

Hydrogen bonds are crucial interactions that significantly contribute to the stability and specificity of protein–ligand interactions. In MD simulations, analyzing the hydrogen bonds formed between the protein and ligand provides valuable insights into the strength and stability of these interactions. Thus, assessing the number and persistence of hydrogen bonds during MD simulations is essential in evaluating the effectiveness of potential drug candidates.

In our study, we analyzed the hydrogen bonds formed by each ligand and the pairs that remained within a distance of 0.35 nm throughout the simulation time. Figure 15 presents the dynamic changes in the number of hydrogen bonds for all the selected complexes. The first

phase space and exhibiting a stable cluster represent more stable complexes, while those occupying a larger space and showing a non-stable cluster correspond to less stable complexes. From the plot, it was observed that LTS0027287 complex occupied a larger space, followed by LTS0205810 and LTS0164686, indicating a less stable cluster compared

Fig. 14 Conformation snapshots of the studied complexes at 0 ns (light green) and 100 ns (yellow) after recentering and rewrapping coordinates

CHEMBL4748063

LTS0078917

LTS0205810

LTS0027287

LTS0131710

LTS0164686

Fig. 15 Number of hydrogen
bonds formed for the trajectory
of molecular dynamics simula-
tions for the selected ligands in
complex with the N-terminus
region of α-synuclein

■ Hydrogen bonds   ■ Pairs within 0.35 nm
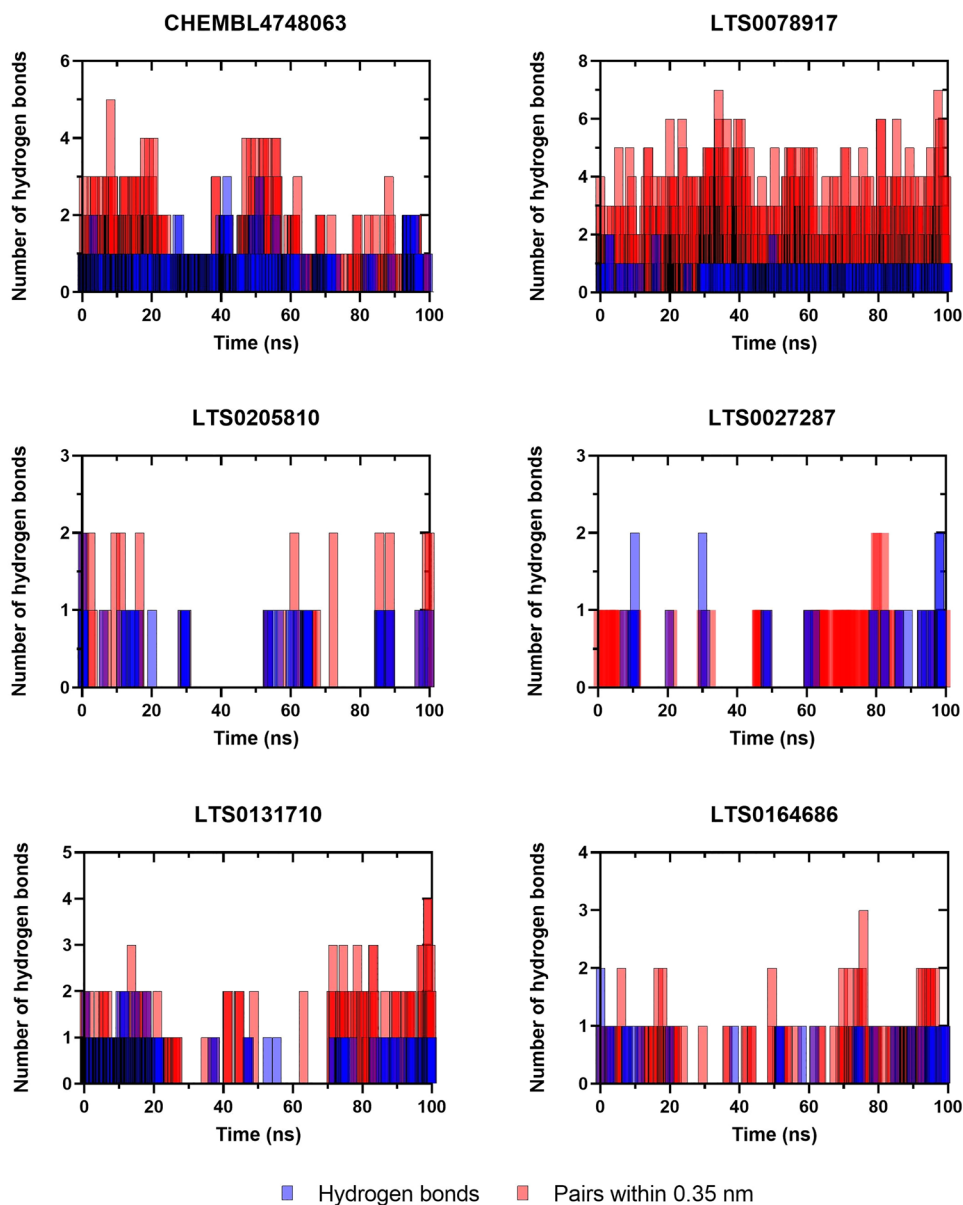
plot reveals that CHEMBL4748063 formed a peak of five
hydrogen bonds within the first 20 ns, leading to one per-
sistent pair within 0.35 nm by the end of the simulation.
Most compounds formed up to three hydrogen bonds.
However, among the ligands investigated, LTS0078917
emerged as the most promising candidate, displaying
notable characteristics in comparison to the other ligands.
In particular, LTS0078917 demonstrated the formation
of up to seven hydrogen bonds, with six consistent pairs
maintained within a distance of 0.35 nm throughout the
entire duration of the simulation. This suggests strong
and stable interactions between LTS0078917 and the tar-
get receptor, making it an intriguing candidate for further
investigation.

Conclusion

Neurodegenerative diseases are associated with protein mis-
folding, which leads to the formation of fibrillar amyloids
and subsequent damage in the brain and other tissues. In
PD, the presence of amyloid fibril aggregates indicates the
abnormal accumulation of the fibrillary protein α-synuclein
in the brain. This accumulation is believed to contribute to
the degeneration of dopamine-producing neurons, resulting
in the motor symptoms of PD. Anle138b shows promise as
a clinical treatment by preventing the formation of amyloi-
dogenic protein aggregates. In this study, we aimed to gain
a deeper understanding of its mechanisms of action, particu-
larly in the N-terminal region of α-synuclein, and identify
potential novel candidates based on natural products using

QSAR and pharmacophore design approaches. Through molecular docking and MD simulations, we found that the studied compounds have the ability to bind to the hairpin like coil region that separates the two α-helices of α-synuclein. By binding to this region, these compounds may hinder conformational changes that lead to the adoption of an elongated shape, which is known to promote the formation and deposition of oligomers. Additionally, since the interhelical region of α-synuclein is involved in lipid binding, compounds targeting this region may prevent the protein from associating to the lipid membranes. Our results highlighted LTS0078917 as a promising candidate, displaying strong binding affinity towards the active site of α-synuclein. The identified natural products may pave the way for further investigation, encompassing the determination of their bioactivity and optimization in the quest for effective PD treatments.

Declarations

Competing interests The authors declare no competing interests.

References

1. Dugger BN, Dickson DW (2017) Pathology of neurodegenerative diseases. Cold Spring Harb Perspect Biol 9(7):a028035
2. Hardy J, Gwinn-Hardy K (1998) Genetic classification of primary neurodegenerative disease. Science 282(5391):1075–1079
3. Goetz CG, Emre M, Dubois B (2008) Parkinson's disease dementia: definitions, guidelines, and research perspectives in diagnosis. Ann Neurol 64(S2):S81–S92
4. Dorsey EA, Constantinescu R, Thompson JP, Biglan KM, Holloway RG, Kieburtz K, Tanner CM (2007) Projected number of people with Parkinson disease in the most populous nations, 2005 through 2030. Neurology 68(5):384–386
5. Wanneveich M, Moisan F, Jacqmin-Gadda H, Elbaz A, Joly P (2018) Projections of prevalence, lifetime risk, and life expectancy of Parkinson's disease (2010–2030) in France. Mov Disord 33(9):1449–1455
6. Martinez-Martin P, Rodriguez-Blazquez C, Paz S, Forjaz MJ, Frades-Payo B, Cubo E, ELEP Group (2015) Parkinson symptoms and health related quality of life as predictors of costs: a longitudinal observational study with linear mixed model analysis. PLoS ONE 10(12):e0145310
7. Chaudhuri KR, Healy DG, Schapira AH (2006) Non-motor symptoms of Parkinson's disease: diagnosis and management. Lancet Neurol 5(3):235–245
8. Jenner P (2003) Oxidative stress in Parkinson's disease. Ann Neurol 53(S3):S26–S38
9. Kalia LV, Kalia SK, Lang AE (2015) Disease-modifying strategies for Parkinson's disease. Mov Disord 30(11):1442–1450
10. Olanow CW, Agid Y, Mizuno Y, Albanese A, Bonucelli U, Damier P, Stocchi F (2004) Levodopa in the treatment of Parkinson's disease: current controversies. Mov Disord 19(9):997–1005
11. Finberg JP (2019) Inhibitors of MAO-B and COMT: their effects on brain dopamine levels and uses in Parkinson's disease. J Neural Transm 126(4):433–448
12. Szabo N, Kincses ZT, Vecsei L (2011) Novel therapy in Parkinson's disease: adenosine A2A receptor antagonists. Expert Opin Drug Metab Toxicol 7(4):441–455
13. Vanle B, Olcott W, Jimenez J, Bashmi L, Danovitch I, IsHak WW (2018) NMDA antagonists for treating the non-motor symptoms in Parkinson's disease. Transl Psychiatry 8(1):1–15
14. Amer DA, Irvine GB, El-Agnaf O (2006) Inhibitors of α-synuclein oligomerization and toxicity: a future therapeutic strategy for Parkinson's disease and related disorders. Exp Brain Res 173(2):223–233
15. Rangasamy SB, Soderstrom K, Bakay RA, Kordower JH (2010) Neurotrophic factor therapy for Parkinson's disease. Prog Brain Res 184:237–264
16. Boulaamane Y, Ibrahim MA, Britel MR, Maurady A (2022) In silico studies of natural product-like caffeine derivatives as potential MAO-B inhibitors/AA2AR antagonists for the treatment of Parkinson's disease. J Integr Bioinform. 19(4):20210027
17. Oliveira L, Gasser T, Edwards R, Zweckstetter M, Melki R, Stefanis L, Outeiro TF (2021) Alpha-synuclein research: defining strategic moves in the battle against Parkinson's disease. Npj Parkinson's Dis 7(1):1–23
18. Das S, Pukala TL, Smid SD (2018) Exploring the structural diversity in inhibitors of α-synuclein amyloidogenic folding, aggregation, and neurotoxicity. Front Chem 6:181
19. Cheng F, Vivacqua G, Yu S (2011) The role of alpha-synuclein in neurotransmission and synaptic plasticity. J Chem Neuroanat 42(4):242–248
20. Takeda A, Mallory M, Sundsmo M, Honer W, Hansen L, Masliah E (1998) Abnormal accumulation of NACP/alpha-synuclein in neurodegenerative disorders. Am J Pathol 152(2):367
21. Gibb WR, Lees A (1988) The relevance of the Lewy body to the pathogenesis of idiopathic Parkinson's disease. J Neurol Neurosurg Psychiatry 51(6):745–752
22. Vicario M, Cieri D, Brini M, Calì T (2018) The close encounter between alpha-synuclein and mitochondria. Front Neurosci 12:388
23. Wagner J, Ryazanov S, Leonov A, Levin J, Shi S, Schmidt F, Giese A (2013) Anle138b: a novel oligomer modulator for disease-modifying therapy of neurodegenerative diseases such as prion and Parkinson's disease. Acta Neuropathologica 125(6):795–813
24. Price DL, Koike MA, Khan A, Wrasidlo W, Rockenstein E, Masliah E, Bonhaus D (2018) The small molecule alpha-synuclein misfolding inhibitor, NPT200-11, produces multiple benefits in an animal model of Parkinson's disease. Sci Rep 8(1):1–12
25. Ulmer TS, Bax A, Cole NB, Nussbaum RL (2005) Structure and dynamics of micelle-bound human α-synuclein. J Biol Chem 280(10):9595–9603
26. Cooper AA, Gitler AD, Cashikar A, Haynes CM, Hill KJ, Bhullar B, Lindquist S (2006) α-Synuclein blocks ER-Golgi traffic and Rab1 rescues neuron loss in Parkinson's models. Science 313(5785):324–328

27. Amos SBT, Schwarz TC, Shi J, Cossins BP, Baker TS, Taylor RJ, Sansom MS (2021) Membrane interactions of α-Synuclein revealed by multiscale molecular dynamics simulations, Markov state models, and NMR. J Phys Chem B 125(11):2929–2941

28. Kondratyev MS, Rudnev VR, Nikolsky KS, Petrovsky DV, Kulikova LI, Malsagova KA, Kaysheva AL (2022) In silico study of the interactions of anle138b isomer, an inhibitor of amyloid aggregation, with partner proteins. Int J Mol Sci 23(24):16096

29. Baul HS, Rajiniraja M (2018) Favorable binding of quercetin to α-synuclein as potential target in Parkinson disease: an insilico approach. Res J Pharm Technol 11(1):203–206

30. Zhu M, Han S, Fink AL (2013) Oxidized quercetin inhibits α-synuclein fibrillization. Biochimica et Biophysica Acta (BBA) 1830(4):2872–2881

31. Ahn TB, Jeon BS (2015) The role of quercetin on the survival of neuron-like PC12 cells and the expression of α-synuclein. Neural Regen Res 10(7):1113

32. Bisi N, Feni L, Peqini K, Pérez-Peña H, Ongeri S, Pieraccini S, Pellegrino S (2021) α-Synuclein: an all-inclusive trip around its structure, influencing factors and applied techniques. Front Chem 9:666585

33. Gaulton A, Bellis LJ, Bento AP, Chambers J, Davies M, Hersey A, Overington JP (2012) ChEMBL: a large-scale bioactivity database for drug discovery. Nucleic acids Res 40(D1):D1100–D1107

34. Bajusz D, Rácz A, Héberger K (2015) Why is Tanimoto index an appropriate choice for fingerprint-based similarity calculations? J Cheminform 7(1):1–13

35. Landrum, G. (2013). RDKit: a software suite for cheminformatics, computational chemistry, and predictive modeling. Greg Landrum

36. Capecchi A, Probst D, Reymond JL (2020) One molecular fingerprint to rule them all: drugs, biomolecules, and the metabolome. J Cheminform 12(1):1–15

37. Rutz A, Sorokina M, Galgonek J, Mietchen D, Willighagen E, Gaudry A, Allard PM (2022) The LOTUS initiative for open knowledge management in natural products research. elife 11:e70780

38. Lipinski CA (2004) Lead-and drug-like compounds: the rule-of-five revolution. Drug Discov Today Technol 1(4):337–341

39. Sander T, Freyss J, von Korff M, Rufener C (2015) DataWarrior: an open-source program for chemistry aware data visualization and analysis. J Chem Inf Model 55(2):460–473

40. Sunseri J, Koes DR (2016) Pharmit: interactive exploration of chemical space. Nucleic Acids Res 44(W1):W442–W448

41. Huey R, Morris GM, Forli S (2012) Using AutoDock 4 and Auto-Dock vina with AutoDockTools: a tutorial. Scripps Res Inst Mol Graphics Lab 10550:92037

42. Volkamer A, Griewel A, Grombacher T, Rarey M (2010) Analyzing the topology of active sites: on the prediction of pockets and subpockets. J Chem Inf Model 50(11):2041–2052

43. Volkamer A, Kuhn D, Grombacher T, Rippmann F, Rarey M (2012) Combining global and local measures for structure-based druggability predictions. J Chem Inf Model 52(2):360–372

44. Trott O, Olson AJ (2010) AutoDock Vina: improving the speed and accuracy of docking with a new scoring function, efficient optimization, and multithreading. J Comput Chem 31(2):455–461

45. Bhakhar KA, Gajjar ND, Bodiwala KB, Sureja DK, Dhameliya TM (2021) Identification of anti-mycobacterial agents against mmpL3: virtual screening, ADMET analysis and MD simulations. J Mol Struct 1244:130941

46. Salentin S, Schreiber S, Haupt VJ, Adasme MF, Schroeder M (2015) PLIP: fully automated protein–ligand interaction profiler. Nucleic Acids Res 43(W1):W443–W447

47. Norinder U, Bergström CA (2006) Prediction of ADMET properties. Chem Enab Drug Discov 1(9):920–937

48. Cheng F, Li W, Liu G, Tang Y (2013) In silico ADMET prediction: recent advances, current challenges and future trends. Curr Top Med Chem 13(11):1273–1289

49. Rao VS, Srinivas K (2011) Modern drug discovery process: an in silico approach. J Bioinform Sequence Anal 2(5):89–94

50. Pires DE, Blundell TL, Ascher DB (2015) pkCSM: predicting small-molecule pharmacokinetic and toxicity properties using graph-based signatures. J Med Chem 58(9):4066–4072

51. Sureja DK, Shah AP, Gajjar ND, Jadeja SB, Bodiwala KB, Dhameliya TM (2022) In-silico computational investigations of antiviral Lignan derivatives as potent inhibitors of SARS CoV-2. ChemistrySelect 7(28):e202202069

52. Van Der Spoel D, Lindahl E, Hess B, Groenhof G, Mark AE, Berendsen HJ (2005) GROMACS: fast, flexible, and free. J Comput Chem 26(16):1701–1718

53. Abraham MJ, Murtola T, Schulz R, Páll S, Smith JC, Hess B, Lindahl E (2015) GROMACS: high performance molecular simulations through multi-level parallelism from laptops to supercomputers. SoftwareX 1:19–25

54. Jo S, Kim T, Iyer VG, Im W (2008) CHARMM-GUI: a web-based graphical user interface for CHARMM. J Comput Chem 29(11):1859–1865

55. Vanommeslaeghe K, MacKerell AD Jr (2012) Automation of the CHARMM General Force Field (CGenFF) I: bond perception and atom typing. J Chem Inf Model 52(12):3144–3154

56. Baammi S, Daoud R, El Allali A (2023) Assessing the effect of a series of mutations on the dynamic behavior of phosphite dehydrogenase using molecular docking, molecular dynamics and quantum mechanics/molecular mechanics simulations. J Biomol Struct Dyn 41(9):4154–4166

57. Gumbart J, Khalili-Araghi F, Sotomayor M, Roux B (2012) Constant electric field simulations of the membrane potential illustrated with simple systems. Biochimica et Biophysica Acta (BBA) 1818(2):294–302

58. Bhandari S, Agrwal A, Kasana V, Tandon S, Boulaamane Y, Maurady A (2022) β-amino carbonyl derivatives: synthesis, molecular docking, ADMET, molecular dynamic and herbicidal studies. ChemistrySelect 7(48):e202201572

59. Boulaamane Y, Ahmad I, Patel H, Das N, Britel MR, Maurady A (2023) Structural exploration of selected C6 and C7-substituted coumarin isomers as selective MAO-B inhibitors. J Biomol Struct Dyn 41(6):2326–2340

60. Vegad UG, Gajjar ND, Nagar PR, Chauhan SP, Pandya DJ, Dhameliya TM (2023) In silico screening, ADMET analysis and MD simulations of phytochemicals of Onosma bracteata wall as SARS CoV-2 inhibitors. 3 Biotech 13(7):221

61. Dhameliya TM, Nagar PR, Gajjar ND (2022) Systematic virtual screening in search of SARS CoV-2 inhibitors against spike glycoprotein: pharmacophore screening, molecular docking, ADMET analysis and MD simulations. Mol Divers 26(5):2775–2792

62. Firth NC, Brown N, Blagg J (2012) Plane of best fit: a novel method to characterize the three-dimensionality of molecules. J Chem Inf Model 52(10):2516–2525

63. Sosnin S, Karlov D, Tetko IV, Fedorov MV (2018) Comparative study of multitask toxicity modeling on a broad chemical space. J Chem Inf Model 59(3):1062–1072

64. Medina-Franco JL, Martínez-Mayorga K, Giulianotti MA, Houghten RA, Pinilla C (2008) Visualization of the chemical space in drug discovery. Curr Comput Aided Drug Des 4(4):322–333

65. Shahapure KR, Nicholas C (2020) Cluster quality analysis using silhouette score. In: 2020 IEEE 7th international conference on data science and advanced analytics (DSAA), pp 747–748. IEEE

66. Rousseeuw PJ (1987) Silhouettes: a graphical aid to the interpretation and validation of cluster analysis. J Comput Appl Math 20:53–65

67. Rosén J, Gottfries J, Muresan S, Backlund A, Oprea TI (2009) Novel chemical space exploration via natural products. J Med Chem 52(7):1953–1962

68. Pollastri MP (2010) Overview on the rule of five. Curr Protoc Pharmacol 49(1):9–12

69. Zhang L, Tan J, Han D, Zhu H (2017) From machine learning to deep learning: progress in machine intelligence for rational drug discovery. Drug Discov Today 22(11):1680–1685

70. Yang J, Hu J, Zhang G, Qin L, Wen H, Tang Y (2021) Pharmacophore modeling and 3D-QSAR study for the design of novel α-synuclein aggregation inhibitors. J Mol Model 27(9):260

71. Vittorio S, Adornato I, Gitto R, Peña-Díaz S, Ventura S, De Luca L (2020) Rational design of small molecules able to inhibit α-synuclein amyloid aggregation for the treatment of Parkinson's disease. J Enzyme Inhib Med Chem 35(1):1727–1735

72. Pettersen EF, Goddard TD, Huang CC, Couch GS, Greenblatt DM, Meng EC, Ferrin TE (2004) UCSF Chimera—a visualization system for exploratory research and analysis. J Comput Chem 25(13):1605–1612

73. Vats S, Kondabala R, Saxena S (2022) Identification of alpha-Synuclein disaggregator from Camellia sp. insight of molecular docking and molecular dynamics simulations. ChemistrySelect 7(10):e202104131

74. Mohankumar T, Chandramohan V, Lalithamba HS, Jayaraj RL, Kumaradhas P, Sivanandam M, Elangovan N (2020) Design and molecular dynamic investigations of 7, 8-dihydroxyflavone derivatives as potential neuroprotective agents against alpha-synuclein. Sci Rep 10(1):599

75. Boulaamane Y, Kandpal P, Chandra A, Britel MR, Maurady A (2023) Chemical library design, QSAR modeling and molecular dynamics simulations of naturally occurring coumarins as dual inhibitors of MAO-B and AChE. J Biomol Struct Dyn 1–18

76. Kufareva I, Abagyan R (2012) Methods of protein structure comparison. Homol Model 231–257

77. Taidi L, Maurady A, Britel MR (2022) Molecular docking study and molecular dynamic simulation of human cyclooxygenase-2 (COX-2) with selected eutypoids. J Biomol Struct Dyn 40(3):1189–1204

78. Durham E, Dorr B, Woetzel N, Staritzbichler R, Meiler J (2009) Solvent accessible surface area approximations for rapid and accurate protein structure prediction. J Mol Model 15:1093–1108

79. Haider S, Parkinson GN, Neidle S (2008) Molecular dynamics and principal components analysis of human telomeric quadruplex multimers. Biophys J 95(1):296–311

80. David CC, Jacobs DJ (2014) Principal component analysis: a method for determining the essential dynamics of proteins. Protein Dyn 193–226

Terms and Conditions

Springer Nature journal content, brought to you courtesy of Springer Nature Customer Service Center GmbH ("Springer Nature").

Springer Nature supports a reasonable amount of sharing of research papers by authors, subscribers and authorised users ("Users"), for small-scale personal, non-commercial use provided that all copyright, trade and service marks and other proprietary notices are maintained. By accessing, sharing, receiving or otherwise using the Springer Nature journal content you agree to these terms of use ("Terms"). For these purposes, Springer Nature considers academic use (by researchers and students) to be non-commercial.

These Terms are supplementary and will apply in addition to any applicable website terms and conditions, a relevant site licence or a personal subscription. These Terms will prevail over any conflict or ambiguity with regards to the relevant terms, a site licence or a personal subscription (to the extent of the conflict or ambiguity only). For Creative Commons-licensed articles, the terms of the Creative Commons license used will apply.

We collect and use personal data to provide access to the Springer Nature journal content. We may also use these personal data internally within ResearchGate and Springer Nature and as agreed share it, in an anonymised way, for purposes of tracking, analysis and reporting. We will not otherwise disclose your personal data outside the ResearchGate or the Springer Nature group of companies unless we have your permission as detailed in the Privacy Policy.

While Users may use the Springer Nature journal content for small scale, personal non-commercial use, it is important to note that Users may not:

1. use such content for the purpose of providing other users with access on a regular or large scale basis or as a means to circumvent access control;

2. use such content where to do so would be considered a criminal or statutory offence in any jurisdiction, or gives rise to civil liability, or is otherwise unlawful;

3. falsely or misleadingly imply or suggest endorsement, approval , sponsorship, or association unless explicitly agreed to by Springer Nature in writing;

4. use bots or other automated methods to access the content or redirect messages

5. override any security feature or exclusionary protocol; or

6. share the content in order to create substitute for Springer Nature products or services or a systematic database of Springer Nature journal content.

In line with the restriction against commercial use, Springer Nature does not permit the creation of a product or service that creates revenue, royalties, rent or income from our content or its inclusion as part of a paid for service or for other commercial gain. Springer Nature journal content cannot be used for inter-library loans and librarians may not upload Springer Nature journal content on a large scale into their, or any other, institutional repository.

These terms of use are reviewed regularly and may be amended at any time. Springer Nature is not obligated to publish any information or content on this website and may remove it or features or functionality at our sole discretion, at any time with or without notice. Springer Nature may revoke this licence to you at any time and remove access to any copies of the Springer Nature journal content which have been saved.

To the fullest extent permitted by law, Springer Nature makes no warranties, representations or guarantees to Users, either express or implied with respect to the Springer nature journal content and all parties disclaim and waive any implied warranties or warranties imposed by law, including merchantability or fitness for any particular purpose.

Please note that these rights do not automatically extend to content, data or other material published by Springer Nature that may be licensed from third parties.

If you would like to use or distribute our Springer Nature journal content to a wider audience or on a regular basis or in any other manner not expressly permitted by these Terms, please contact Springer Nature at

onlineservice@springernature.com